ACS OMEGA

Article

Cite This: ACS Omega 2018, 3, 14266−14273

http://pubs.acs.org/journal/acsodf

Antiferromagnetic Interfacial Coupling and Giant Magnetic Hysteresis in $La_{0.5}Ca_{0.5}MnO_3$−$SrRuO_3$ Superlattices

Vandrangi Suresh Kumar,[†,‡,◆] Shu-Liang Zhou,[†,◆] Rui-Rui Liu,[†] Yuan-Min Zhu,[†,§] Heng-Jui Liu,[∥] Yi-Ying Chin,[⊥] Hong-Ji Lin,[#] Chien-Te Chen,[#] Qian Zhan,*[,†] and Ying-Hao Chu*[,∇,○]

[†]School of Materials Science and Engineering, University of Science and Technology Beijing, Xueyuan Road 30, 100083 Beijing, China

[‡]School of Advanced Sciences, Vellore Institute of Technology, 632014 Vellore, India

[§]Department of Materials Science and Engineering and Academy for Advanced Interdisciplinary Studies, Southern University of Science and Technology of China, No. 1088, Xueyuan Road, 518055 Shenzhen, China

[∥]Department of Materials Science and Engineering, National Chung Hsing University, 145 Xingda Road, 40227 Taichung, Taiwan

[⊥]Department of Physics, National Chung Cheng University, No. 168, Section 1, University Road, Minhsiung Township, 62102 Chiayi, Taiwan

[#]National Synchrotron Radiation Research Center, 101 Hsin-Ann Road, 30076 Hsinchu, Taiwan

[∇]Department of Materials Science and Engineering, National Chiao Tung University, 1001 University Road, 30010 Hsinchu, Taiwan

[○]Institute of Physics, Academia Sinica, Section 2, Academia Road, Nangang district, 11529 Taipei, Taiwan

ABSTRACT: Superlattices are of great importance due to their potential as new materials genome to synthesize new functional materials. Thus, tuning of the ground state of superlattices is crucial to further control their physical properties. In this study, superlattices (SLs) consisting of alternating layers of $SrRuO_3$ (SRO) (5 nm) and $La_{0.5}Ca_{0.5}MnO_3$ (LCMO) (5 nm) are epitaxially grown on $SrTiO_3$ (STO) and $LaAlO_3$ (LAO) substrates with 10-unit-cell periods. A variation in the substrate-induced-strain for this choice of SLs triggers observation of remarkable properties, such as magnetic anisotropy and large magnetic hysteresis. The strain states experienced by LCMO and SRO in these SLs result in strong ferromagnetic interlayer coupling and weak antiferromagnetic interlayer coupling at low temperatures in SLs of LCMO−SRO/STO and a strong antiferromagnetic interlayer coupling in SLs of LCMO−SRO/LAO. Besides, a large magnetic hysteresis resulting from the predominant magnetic anisotropy of SRO together with the strength of magnetic coupling is observed in SLs of LCMO−SRO/LAO along the out-of-plane direction of the LAO substrate. These four different magnetic behaviors along four different directions of substrate orientations are interpreted in terms of preferential orbital occupation and competing magnetic exchange coupling together with magnetic anisotropy. This study demonstrates the subtleties in controlling the strength of magnetic coupling at the interface and stands as a model system to realize fascinating magnetic phenomena in layer-by-layer hetero-epitaxial oxide films.

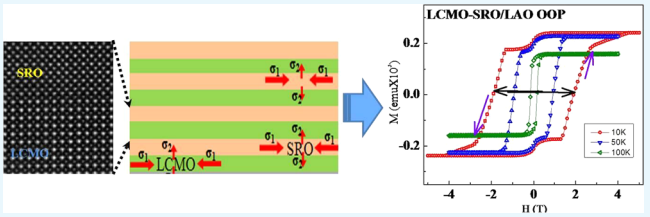

INTRODUCTION

Magnetic phenomena emerging from the interface of oxide materials never cease to astonish with their remarkable properties, when there is a unique way of[1,2] manipulating the interface.[3,4] They are the key dictators of modern technological development. To keep up the pace at which the progress in various areas is being advanced, an increasing demand has to be handled by exploring[5] and exploiting new possibilities in terms of understanding the complexity of interfaces and materials for technology. In this connection, producing exotic magnetic phenomena at the interface using strain as one of the control parameters in self-assembled heterostructure systems is a formidable task and when reasonably achieved, it is considered to be an appreciable contribution to the science and technology. In the process of accomplishing this, magnetic heterostructures fabricated with the help of state-of-the-art techniques, creating sharp interfaces with atomic precision, have been a topic of great interest and offer an avenue to tune and tailor different magnetic interactions by the choice of materials like manganites and ruthenates when they are put in the form of bilayers,[6,7] trilayers,[8] heterostructures,[9,10] and nanocomposites.[11] The most attractive attributes commonly noticed in different forms of material structures are the nature of magnetic coupling and the strength of magnetic coupling at

Received: August 3, 2018
Accepted: October 12, 2018
Published: October 29, 2018

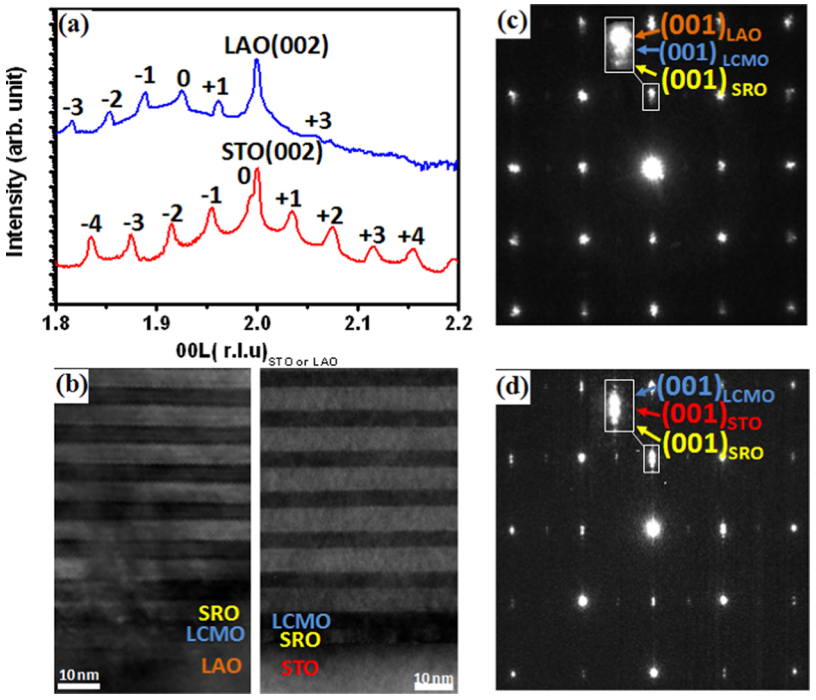

Figure 1. (a) Out-of-plane (OOP) XRD profiles of LCMO−SRO SLs epitaxially grown on STO(001) and LAO(001) were recorded and represented by red and blue curves, respectively. The Bragg reflections of substrates as well as the satellite peaks of the superlattice are indicated. (b) Low-magnification diffraction-contrast cross-sectional TEM image of the SLs grown on STO and LAO substrates; alternating bright and dark layers are SRO and LCMO layers, respectively. (c, d) Selected area EDPs of the SLs epitaxially grown on LAO and STO in the cross-section sample along the [100] zone axis, respectively.

the interface. The complexity of magnetic order, resulting from the above-mentioned factors, mainly depends on the dominant energy of Zeeman, exchange coupling, and anisotropy terms. Hence, how well we deal with the complexity of magnetic order in a system matters a lot, in producing magnetic properties of immense potential.

Persuaded by the luxury to tune magnetic properties of complex oxide heterostructures because of the significant interplay among energy terms, in this work, we demonstrate an attempt to create diverse magnetic behaviors in magnetic SLs without the aid of external stimuli but by choosing a particular size of constituent layers of $La_{0.5}Ca_{0.5}MnO_3$ (LCMO) and $SrRuO_3$ (SRO), and substrates $SrTiO_3$ (STO) and $LaAlO_3$ (LAO). The charge ordering in LCMO can be destabilized when it is in the form of thin films, and in the process of destabilizing the charge ordered state, we anticipate that both ferromagnetic and antiferromagnetic phases will be present. This would be of help to produce remarkable properties when combined with SRO. The selection of substrates is made in such a way that SRO experiences strain in both the cases, whereas LCMO undergoes strain in only one case (on STO). It is further identified that fabrication of sublayers with increasing thickness is possible for STO; however, it is not quite easy for LAO because the lattice mismatch between SRO and LAO is very large. Hence, we preferred the thickness of the sublayers to be below the critical thickness for SRO grown on a LAO substrate (5 nm), so as to maintain the surface/interface smoothness. With this approach, we find that it is possible to control the competing energies, in particular, exchange coupling and magnetic anisotropy, and create complementary magnetic behaviors (soft and hard) in these SLs as a function of substrate orientation. This study throws light on the diversity of creating dominant ferromagnetic/antiferromagnetic couplings and soft or hard magnetic behaviors in magnetic SLs.

RESULTS AND DISCUSSION

The X-ray diffraction (XRD) for SLs epitaxially grown on STO and LAO along the surface direction is shown in Figure 1a. Both samples have high quality and a periodic modulation of the two constituent phases that can be clearly identified by the presence of regularly distributed high-order satellite peaks around the main peak (zeroth order) of SLs. The presence of well-aligned (00*l*) diffraction peaks of the SLs gives the orientation relationship between SLs and the substrates, STO and LAO: SRO[001]//LCMO[001]//STO[001]; SRO[001]//LCMO[001]//LAO[001], demonstrating good epitaxy with *c*-axis orientation between SLs and the substrate. Moreover, the homologous modulation length ($\Lambda = a_{sub}/\Delta L$) of SLs grown on LAO and STO is estimated to be around 10 nm in conformity with the originally designed thickness.[5] ΔL is the interval between two neighboring thickness fringes. Because L is the reciprocal lattice normalized by the substrate lattice, the length or thickness in real space can be determined by the inverse of the spacing (ΔL) between two neighboring interference peaks multiplied by the substrate lattice constant. The concept is widely used in many diffraction techniques, such as XRD, transmission electron microscopy (TEM), etc.

Relevant information concerning the heterointerface structure of the superlattice and its epitaxial relationship can be obtained from TEM analysis. The low-magnification images of the films grown on LAO (left) and STO (right), shown in Figure 1b, exhibit sharp, flat, and well-defined interfaces between alternate SRO (bright contrast) and LCMO (dark contrast) layers. Both superlattices are periodically stacked on different substrates with an individual periodic sublayer

DOI: 10.1021/acsomega.8b01851
ACS Omega 2018, 3, 14266−14273

thickness of ∼10 nm in both systems, which is in good agreement with the above XRD results. Considering the lattice matching degree, the LCMO layer is deposited first, and then the SRO layer on the LAO substrate, whereas SRO is deposited first, and LCMO later on the STO substrate. Thus, the inverse contrast of the initially deposited sublayer is observed in different substrates. The corresponding electron diffraction pattern (Figure 1c,d) confirms the *c*-axis orientation of the films and the orientation relationships are determined: $(001)_{SRO} \| (001)_{LCMO} \| (001)_{LAO/STO}$; $[100]_{SRO} \| [100]_{LCMO} \| [100]_{LAO/STO}$.

Figure 2 gives the high-angle annular dark field-scanning transmission electron microscopy (HADDF-STEM) image of

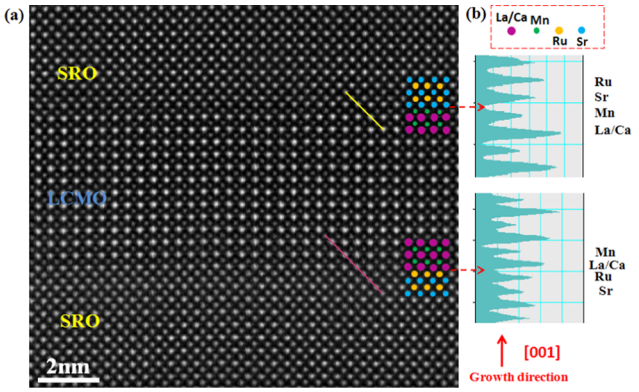

Figure 2. (a) Z-STEM micrograph of LCMO−SRO SL showing the interfaces between a 5 nm LCMO layer and two adjacent 5 nm thin SRO layers. (b) Intensity scan along the yellow and purple lines as indicated in (a).

the LCMO−SRO SLs taken using a JEM-ARM200F TEM incorporated with a STEMCs corrector, revealing the bonding characteristic of the heterointerface structure. The HADDF-STEM image demonstrates an atomic number *Z* contrast that is roughly proportional to the square of the atomic number *Z* (Z^2).[12] It is, thereby, believed that different intensities can represent different atomic columns directly. Thus, it is easy to conclude that the brighter and darker dots represent La/Ca (57/20) and Mn(25) columns, respectively, in the LCMO layer, the bright and dark dots represent Ru(44) and Sr(38) columns, respectively, in the SRO layers (Figure 2a). The line scan profiles including all typical atoms across the interface between SRO and LCMO layers were performed, and the results are given in Figure 2b, as indicated by the yellow and purple lines in Figure 2a. It is largely terminated with the BO_2 plane of each layer along the growth direction in these SLs grown on STO and LAO.

Through the high-precision statistics and calculation on the two-dimensional atomic coordinates with the high-resolution TEM (HRTEM) images, the in-plane (IP) and out-of-plane lattice parameters of the SLs grown on STO and LAO substrates displayed as a function of the distance away from the substrates along the *c*-axis are given in Figure 3. Every data point was obtained by averaging the measured in-plane and out-of-plane values for each row of the individual unit cells parallel to the interface. Figure 3a,b shows the measured values for SRO and LCMO (shadow area) grown on STO substrates along the in-plane and out-of-plane directions, respectively. The in-plane lattice parameters of the superlattice are approximately equal to the bulk value of the STO substrate with a = 0.3905 nm (Figure 3a), suggesting the strong constraint effect of the substrate in the thin film system. Along the out-of-plane direction, the measured value of SRO is larger, whereas it is smaller for LCMO compared with theoretical bulk parameters.

Hence, it is observed that SRO undergoes in-plane compressive strain and out-of-plane tensile strain; meanwhile, LCMO has an in-plane tensile strain and is almost strain free in SLs grown on the STO substrate, from our analysis of the lattice parameters. On the other hand, the strain state of the superlattice grown on the LAO substrate is also investigated in the same way. Surprisingly, sensitive lattice variations are detected only at the first period of the superlattice. As presented in Figure 3c, in-plane parameters of both LCMO and SRO are smaller than those of bulk values at the first period due to the constraint of the LAO substrate (a = 3.79 Å). After the first unit cell, the lattice parameter of LCMO is relaxed and gets very close to the bulk lattice parameter (a = 3.86 Å). Similarly, SRO is also subjected to a compressive stress followed by the increase in parameters due to its own large bulk values in the first period. Then, the lattice parameters of LCMO and SRO have a stable value after the first period till the end of the stacking and are shown in Figure 3d. The values of pseudocubic lattice parameters of SRO and LCMO on STO and LAO substrates are listed in Table 1. The strain states experienced by SRO and LCMO on STO and LAO substrates are clearly depicted with the help of arrows in Figure 3e,f, respectively.

Magnetization as a function of temperature for the SLs grown on STO and LAO substrates, in the temperature ranges 300−10 and 380−10 K, respectively, measured along the in-plane (IP) and out-of-plane (OOP) directions during cooling and heating cycles under a magnetic field of 100 Oe, is plotted in the top panel of Figure 4. LCMO is known to have an atomic force microscopy (AFM) ordering in the bulk but in thin films, an antiferromagnetic-to-ferromagnetic transition is observed with increasing thickness of the LCMO layer.[13] SRO is known to have its T_C around 150 K in the thin film[14] form. It is worth noting that the magnetization behaviors of SLs are completely different in all four crystallographic orientations, namely, along the STO[100] direction (IP-STO), STO[001] direction (OOP-STO), LAO[100] direction (IP-LAO), and LAO[001] direction (OOP-LAO). Along IP-STO, we identify that the Curie temperatures of SRO (∼110 K) and LCMO (∼150 K) are shifted to low temperatures, and these values of Curie temperature are consistent with those of SRO and LCMO single layers on STO (shown in the inset). A peak in magnetization appears around 145 K, for SLs grown on LAO along IP-LAO, indicative of antiferromagnetic coupling. It can be understood, as the LCMO layers order ferromagnetically first and SRO layers start to order ferromagnetically at low temperatures, with their orientation being antiparallel to those of LCMO layers, when the SLs are cooled under an external magnetic field. Such a peak in magnetization is not seen along any other crystallographic orientation, and hence, the antiferromagnetic coupling strength seems to be the strongest for SLs on the LAO substrate. A better understanding of the magnetic interactions between SRO and LCMO layers on STO and LAO substrates is possible from field-dependent magnetization behavior.

Magnetization as a function of the magnetic field, $M(H)$, has been recorded, and the $M(H)$ curves along the out-of-plane orientation of SLs grown on STO and LAO in the temperature

DOI: 10.1021/acsomega.8b01851
ACS Omega 2018, 3, 14266−14273

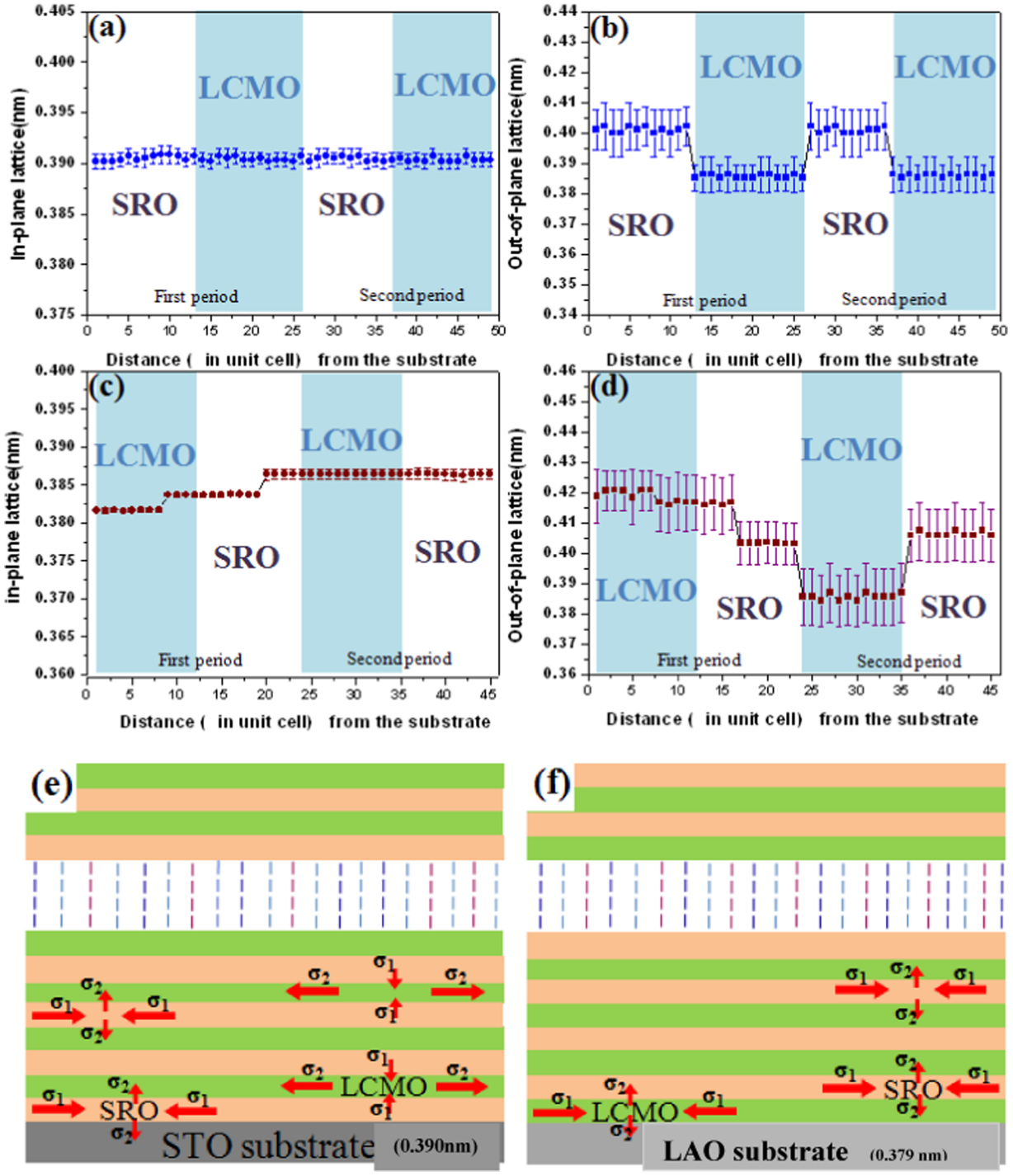

Figure 3. (a) and (b) are the in-plane and out-of-plane lattice parameters of the superlattice near the STO substrate, respectively, that are displayed as a function of the distance along the *c*-axis of the substrate. (c) and (d) are the in-plane and out-of-plane lattice parameters of the superlattice near the LAO substrate, respectively, that are displayed as a function of the distance along the *c*-axis of the substrate. (e) and (f) are the stress distribution of the SLs grown on STO and LAO, respectively, in the two-dimensional space.

range 100−10 K are shown in the bottom panel of Figure 4. Here, the competition between Zeeman energy and energy of AF coupling is expected to play an important role, i.e., at high magnetic fields, Zeeman energy is predominant, and at low magnetic fields, the energy of antiferromagnetic interlayer coupling exceeds the Zeeman energy. The competition between these two energies has been reflected in the $M(H)$ curves for IP-LAO and, on the other hand, there is no signature of AF coupling in the case of IP-STO (not shown here), as the same can be observed from the $M(T)$ curves. Remarkably, $M(H)$ behaviors along OOP-STO and OOP-LAO are striking in terms of AF coupling and magnetic hysteresis, respectively. $M(H)$ for OOP-STO shows hard axis behavior and magnetization switching behavior. The switching is an obvious sign of antiferromagnetic interlayer coupling between the two component layers. The shape of the step in the $M(H)$ loop is understood based on the magnetic moments of the layers. As LCMO has a higher magnetic moment compared to

DOI: 10.1021/acsomega.8b01851
ACS Omega 2018, 3, 14266−14273

Table 1. Lattice Parameters of SRO and LCMO Layers in the Superlattices along IP and OOP Directions of STO and LAO Substrates Together with Their Bulk Counterparts and Also STO and LAO Substrates

sample	bulk (nm)	IP-STO (nm)	OOP-STO (nm)	IP-LAO (nm)	OOP-LAO (nm)
SRO	0.394	0.390	0.4	0.387	0.405
LCMO	0.386	0.390	0.385	0.387	0.385
STO	0.390				
LAO	0.379				

SRO, it saturates first and the second step is contributed by SRO. The coercive field measured from $M(H)$ loops attains the highest value of ∼ 800 Oe around 50 K. The OOP-LAO magnetic loops show large magnetic coercive fields due to strong magnetic anisotropy of SRO layers that shows up at low temperatures. The magnitude of the hysteresis loop at 10 K is as large as 4 T, which is much larger than that of the SRO component layer. This kind of hysteresis is rarely observed in manganite−ruthenite magnetic SLs. Besides, magnetization switching behavior is present similar to that in the OOP-STO configuration but only observed at low temperatures. The complexity of magnetic order is mainly governed by the magnetic competition among AF interlayer coupling, magnetic anisotropy, and Zeeman effect.

To detect the contrasting magnetization behaviors of the SLs on STO and LAO substrates, we employed two complementary and powerful[15] techniques, X-ray linear dichroism (XLD) and X-ray magnetic circular dichroism (XMCD). The Mn dichroism spectra for LCMO−SRO/STO and LCMO−SRO/LAO superlattices, obtained as the difference between the X-ray absorption spectroscopy (XAS) data taken with the helicity parallel and antiparallel to the applied magnetic field ($E//ab$ and $E//c$), in the temperature ranges 300−50 and 200−50 K, respectively, are shown in the top panel of Figure 5. The two major contributions to Mn dichroism spectra are magnetic and orbital occupation. At temperatures below the magnetic transition temperature, a strong magnetic contribution to Mn dichroism spectra is expected, whereas above the magnetic transition temperatures, the only contribution to dichroism spectra comes from the preferential orbital occupation. There is no considerable change in the intensities of these dichroism spectra for SLs grown on STO above 150 K. The changes in the intensity and shape of the spectra are clearly observed at temperatures close to 50 K. We understand that with decreasing temperature, the AFM phase starts to appear at temperatures below 100 K, and this appearance and change in the AFM phase are also depicted in the magnetic phase transitions observed from temperature- and field-dependent magnetization curves. On the other hand, the observed change is rather significant, particularly between the temperatures 100 and 50 K, in the case of SLs grown on LAO. This considerable change in the intensity of dichroism spectra is attributed to the presence of a larger antiferromagnetic phase in SLs grown on LAO compared to those grown on STO. We see that the temperature range over which the AFM phase evolves closely matches with the temperate range over which the phase transitions are observed in $M(T)$ behavior. The magnetic phases here are driven by strain-induced structural deformation and can be addressed in terms of preferential orbital occupation among Mn and Ru ions[16] at the interface, as orbital hybridization and strain-dependent orbital occupation have key roles to play in deciding the interfacial magnetic coupling. The observed difference in the shape of these dichroism spectra with temperature hints that the orientation of the local magnetic moment of the corresponding dominant magnetic phase changes with temperature and further

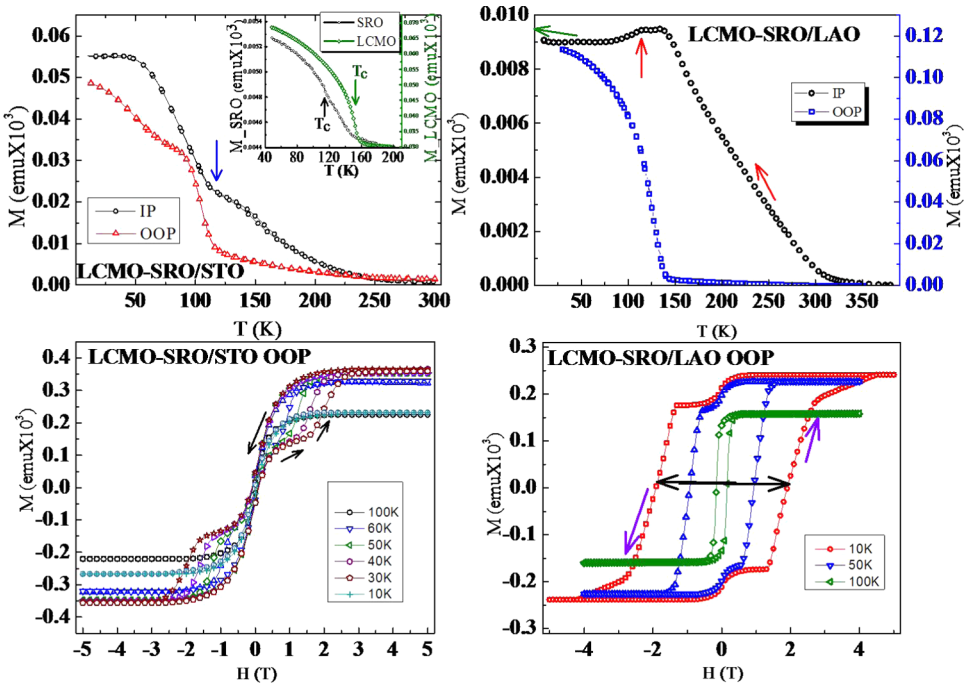

Figure 4. Temperature dependence of magnetization along IP and OOP directions for LCMO−SRO/STO and LCMO−SRO/LAO under a magnetic field of 100 Oe (top panel). OOP magnetization loops, $M(H)$, for the SLs grown on STO and LAO (bottom panel) at temperatures around the magnetic anomalies and at 10 K. Inset: temperature-dependent magnetization for SRO (5 nm) and LCMO (5 nm) on STO.

DOI: 10.1021/acsomega.8b01851
ACS Omega 2018, 3, 14266−14273

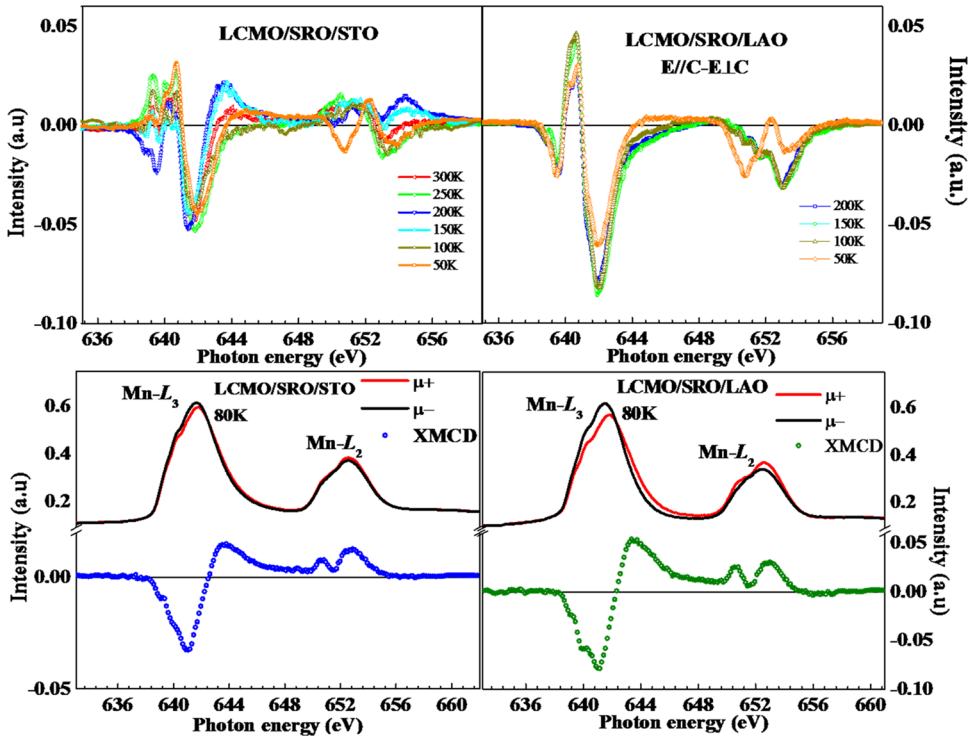

Figure 5. (Top panel) Mn$L_{2,3}$-edge linear dichroism ($E//ab-E//c$) of LCMO−SRO superlattice samples grown on STO and LAO, in the temperature ranges 300−50 and 200−50 K, respectively. (bottom panel) Mn$L_{2,3}$-edge XMCD of LCMO−SRO superlattice samples recorded at 80 K grown on STO and LAO.

contributes to magnetic anisotropy. The lower panel of Figure 5 depicts the XMCD spectra for LCMO−SRO/STO SLs and LCMO−SRO/LAO SLs recorded at 80 K. The larger signal in SLs grown on LAO compared to that in SLs grown on STO shows that spin orientation depends on the substrate. Importantly, the magnetic hysteresis in this case is remarkably large.

It is well known that structural deformation determines the stabilization of either in-plane $e_g(x^2 - y^2)$ or out-of-plane $e_g(3z^2 - r^2)$ orbital order.[17] In the present case, the XLD spectra provide an understanding of the preferred orbital occupation in the SLs grown on STO and LAO that the expansion of the in-plane lattice parameter of LCMO in LCMO−SRO/STO SLs results in a decrease in the Mn−O bond length and the preferential occupation would be a mixture of the IP $x^2 - y^2$ orbital and OOP $(3z^2 - r^2)$ orbital. On the other hand, a slight expansion of the out-of-plane lattice parameter of LCMO in LCMO−SRO/LAO SLs and a probable increase in the Mn−O bond length favor occupation of the IP $x^2 - y^2$ orbital.

It is important to note here that, in accordance with Goodenough−Kanamori rules, the empty e_g orbitals in Ru of SRO can ferromagnetically couple with partially filled e_g orbitals of Mn^{3+} but antiferromagnetically couple with Mn^{4+} of LCMO at the interface, as there are no e_g electrons available in Mn^{4+}. In LCMO, even though equal number of Mn^{3+} and Mn^{4+} ions are available, the same may not reflect in the availability of partially filled or empty e_g orbitals, mainly because of the fact that orbital filling depends on the amount of strain experienced by LCMO and SRO at the interface. This strain mainly controls the relative energies of the t_{2g} orbitals of Mn and Ru. Under these conditions, an e_g electron of Ru easily hops between Ru and Mn ions in SLs grown on STO, as the energy difference associated with the transfer process is small, giving rise to dominant FM coupling, whereas this energy difference must be larger for SLs grown on LAO, resulting in AF coupling. Besides, we see two contributions to magnetic anisotropy, one comes from the reduced symmetry at the interface, resulting from the modification of surface energy, and the second comes from the distortion of the lattice because of the strain between magnetic layers, resulting from the modification of volume energy. SRO is known for its large magnetic anisotropy[18] depending on the strain it undergoes. In the current study, LCMO and SRO play crucial roles of tuning the strength of the magnetic coupling (FM and AF) at the interface and the competition between magnetic coupling and magnetic anisotropy in producing a large magnetic hysteresis by merely changing the orientation and the substrate.

CONCLUSIONS

To summarize, SLs of LCMO−SRO/STO and LCMO−SRO/LAO show diverse magnetic properties along different orientations of the substrates. These remarkable properties are mainly attributed to the competition between magnetic coupling and magnetic anisotropy at the interface, resulting from the substrate-induced strain states experienced by the constituent magnetic layers. SLs of LCMO−SRO exhibit mainly FM interlayer coupling on STO substrates and AFM coupling on LAO substrates. A large magnetic hysteresis, resulting from the predominant magnetic anisotropy of SRO together with magnetic coupling, is observed in SLs of LCMO−SRO/LAO along the OOP direction of LAO substrates. The strain states experienced by LCMO and SRO in SLs contribute to strong AF coupling as a consequence of preferential orbital occupation, and on the other hand, the magnetic anisotropy of SRO is enhanced to give rise to a large

DOI: 10.1021/acsomega.8b01851
ACS Omega 2018, 3, 14266−14273

magnetic hysteresis along the OOP direction. This study makes a profound impact in the field of magnetic heterostructures by providing the freedom to select between complementary magnetic behaviors in the same SLs.

EXPERIMENTAL DETAILS

Sample Fabrication. The LCMO−SRO superlattices were fabricated artificially on single-crystalline (001)-oriented STO and LAO substrates by pulsed-laser deposition. Single-terminated and atomically flat surfaces of STO and LAO are obtained by a typical chemical treatment and an annealing process[19] and only high-temperature annealing,[20] respectively. The growth process was carried out at 700 °C under an oxygen partial pressure of 100 mTorr. Ten-period layers were grown with the alternation of 5 nm-thick SRO and 5 nm-thick LCMO. The accurate thickness of SLs together with a layer-by-layer growth mode was monitored in situ by reflection high-energy electron diffraction.

Transmission Electron Microscopy. The lattice structures of the high-quality LCMO−SRO SLs were successfully evidenced and analyzed by X-ray diffraction (XRD) and transmission electron microscopy (TEM). The high-resolution scanning transmission electron microscopy (HR-STEM) experiments were carried on a JEM-ARM200, which was operated at 200 keV with a cold field-emission electron gun having a resolution of 0.078 nm. The HRTEM investigations were performed in a TITAN 80-300 FEI microscope with a spherical aberration-corrected probe-forming system. The cross-section specimens suitable for TEM observations were prepared via a standard procedure followed by the mechanical grinding, polishing and ion beam milling processes.

Magnetic Measurements and Analysis. To determine the magnetic ordering and the magnetic coupling between SRO and LCMO layers, a Quantum Design Magnetic Property Measurement System (MPMS) Superconducting Quantum Interference Device (SQUID) magnetometer was employed.

X-ray Absorption Spectroscopy. Element-specific X-ray absorption spectroscopy (XAS) and X-ray magnetic linear and circular dichroism (XMCD and XMLD) measurements were performed at *L*-edges of Mn to carefully study the electronic and spin states of Mn ions in these heterostructures. The XMCD and XMLD spectra were recorded in total electron yield mode at the Dragon beamline at the National Synchrotron Radiation Research Center, Taiwan.

AUTHOR INFORMATION

Corresponding Authors

*E-mail: qzhan@mater.ustb.edu.cn (Q.Z.).
*E-mail: yhchu@g2.nctu.edu.tw (Y.-H.C.).

ORCID

Yuan-Min Zhu: 0000-0001-9554-3005
Heng-Jui Liu: 0000-0002-0745-9370
Ying-Hao Chu: 0000-0002-3435-9084

Author Contributions

◆V.S.K. and S.-L.Z. contributed equally to this work.

Notes

The authors declare no competing financial interest.

ACKNOWLEDGMENTS

This work was supported by the National Natural Science Foundation of China with Grant Nos. 51571021 and 51371031.

REFERENCES

(1) Ke, X.; Rzchowski, M. S.; Belenky, L. J.; Eom, C. B. Positive Exchange Bias in Ferromagnetic $La_{0.67}Sr_{0.33}MnO_3/SrRuO_3$ Bilayers. *Appl. Phys. Lett.* **2004**, *84*, 5458.

(2) Solignac, A.; Guerrero, R.; Gogol, P.; Maroutian, T.; Ott, F.; Largeau, L. L.; Lecoeur, P. H.; Pannetier-Lecoeur, M. Dual Antiferromagnetic Coupling at $La_{0.67}Sr_{0.33}MnO_3/SrRuO_3$ interfaces. *Phys. Rev. Lett.* **2012**, *109*, No. 027201.

(3) Skinner, T. D.; Kurebayashi, H.; Fang, D.; Heiss, D.; Irvine, A. C.; Hindmarch, A. T.; Wang, M.; Rushforth, A. W.; Ferguson, A. J. Enhanced Inverse Spin-Hall Effect in Ultrathin Ferromagnetic/normal Metal Bilayers. *Appl. Phys. Lett.* **2013**, *102*, No. 072401.

(4) Guo, E.-J.; Charlton, T.; Ambaye, H.; Desautels, R. D.; Lee, H. N.; Fitzsimmons, M. R. Orientation Control of Interfacial Magnetism at $La_{0.67}Sr_{0.33}MnO_3/SrTiO_3$ interfaces. *ACS Appl. Mater. Interfaces* **2017**, *9*, 19307.

(5) Liu, H. -J; Wei, T.-C.; Zhu, Y.-M.; Liu, R.-R.; Tzeng, W.-Y.; Tsai, C.-Y.; Zhan, Q.; Luo, C.-W.; Yu, P.; He, J.-H.; Chu, Y.-H.; He, Q. Strain-Mediated Inverse Photoresistivity in $SrRuO_3/La_{0.7}Sr_{0.3}MnO_3$ Superlattices. *Adv. Funct. Mater.* **2016**, *26*, 729.

(6) Ke, X.; Belenky, L. J.; Lauter, V.; Ambaye, H.; Bark, C. W.; Eom, C. B.; Rzchowski, M. S. Spin Structure in an Interfacially Coupled Epitaxial Ferromagnetic Oxide Heterostructures. *Phys. Rev. Lett.* **2013**, *110*, No. 237201.

(7) Ding, J. F.; Lebedev, O. I.; Turner, S.; Tian, Y. F.; Hu, W. J.; Seo, J. W.; Panagopoulus, C.; Prellier, W.; Van Tendeloo, G.; Wu, T. Interfacial Spin Glass State and Exchange Bias in Manganite Bilayers With Competing Magnetic Orders. *Phys. Rev. B* **2013**, *87*, No. 054428.

(8) Seo, J. W.; Prellier, W.; Padhan, P.; Boullay, P.; Kim, J.-Y.; Lee, H.; Batista, C. D.; Martin, I.; Chia, E. M.; Wu, T.; Cho, B.-G.; Panagopoulos, C. Tunable Magnetic Interactions at the Atomic Scale in Oxide Heterostructures. *Phys. Rev. Lett.* **2010**, *105*, No. 167206.

(9) Shiomi, Y.; Handa, Y.; Kikkawa, T.; Saitoh, E. Anamalous Hall Effect with Giant Hysteresis Loop in $La_{0.67}Sr_{0.33}MnO_3/SrRuO_3$ Superlattices. *Phys. Rev. B* **2015**, *92*, No. 024418.

(10) Singamaneni, S. R.; Wu, F.; Prater, J. T.; Narayan, J. Complete Vertical M-H loop Shift in $La_{0.67}Sr_{0.33}MnO_3/SrRuO_3$ Thin-film Heterostructures. *J. Appl. Phys.* **2015**, *117*, No. 17B711.

(11) Vandrangi, S. K.; Yang, J.-C.; Zhu, Y.-M.; Chin, Y.-Y.; Lin, H.-J.; Chen, C.-T.; Zhan, Q.; He, Q.; Chen, Y.-C.; Chu, Y.-H. Enhanced Magnetocaloric Effect Driven by Interfacial Magnetic Coupling in Self-Assembled Mn_3O_4-$La_{0.7}Sr_{0.3}MnO_3$ Nanocomposites. *ACS Appl. Mater. Interfaces* **2015**, *7*, 26504.

(12) Okunishi, E.; Sawada, H.; Kondo, Y. Experimental Study of Annular Bright Field (ABF) Imaging Using Aberration-corrected Scanning Transmission Electron Microscopy (STEM). *Micron* **2012**, *43*, 538.

(13) Padhan, P.; Prellier, W. Exchange-coupling-induced Antiferromagnetic-ferromagnetic Transition in $Pr_{0.5}Ca_{0.5}MnO_3/La_{0.5}Ca_{0.5}MnO_3$ Superlattices. *Phys. Rev. B* **2005**, *71*, No. 174419.

(14) Vailionis, A.; Siemons, W.; Koster, G. Room Temperature Epitaxial Stabilization of a Tetragonal Phase in $ARuO_3$ (A = Ca and Sr) Thin-films. *Appl. Phys. Lett* **2008**, *93*, No. 051909.

(15) Nolting, F.; Scholl, A.; Stohr, J.; Seo, J. W.; Fompeyrine, J.; Siegwart, H.; Locquet, J.-P; Anders, S.; Luning, J.; Fullerton, E. E.; Toney, M. F.; Scheinfein, M. R.; Padmore, H. A. Direct Observation of the Alignment of Ferromagnetic Spins by Antiferromagnetic Spins. *Nature* **2000**, *405*, 767.

(16) May, S. J.; Kim, J. W.; Rondinelli, J. M.; Karapetrova, E.; Spaldin, N. A.; Bhattacharya, A.; Ryan, P. J. Quantifying Octahedral Rotations in Strained Perovskite Oxide Films. *Phys. Rev. B* **2010**, *82*, No. 014110.

(17) Abad, L.; Laukhin, V.; Valencia, S.; Gaup, A.; Gudat, W.; Balcells, L.; Martinez, B. Interfacial Strain: The Driving Force for Selective Orbital Occupancy in Manganite Thin Films. *Adv. Funct. Mater.* **2007**, *17*, 3918.

(18) Koster, G.; Klein, L.; Siemons, W.; Rijnders, G.; Dodge, J. S.; Eom, C.-B.; Blank, D. H. A.; Beasley, M. R. Structure, Physical

DOI: 10.1021/acsomega.8b01851
ACS Omega 2018, 3, 14266−14273

Properties, and Applications of $SrRuO_3$ Thin Films. *Rev. Mod. Phys.* **2012**, *84*, 253.
(19) Koster, G.; Kropman, B. L.; Rijnders, J. H. M.; Blank, D. H. A.; Rogalla, H. Quasi-ideal strontium titanate crystal surfaces through formation of strontium hydroxide. *Appl. Phys. Lett.* **1998**, *73*, 2920.
(20) Liu, Z. Q.; Huang, Z.; Lu, W. M.; Gopinadhan, K.; Wang, X.; Annadi, A.; Venkatesan, T.; Ariando. Atomically flat interface between a single-terminated LaAlO3 substrate and SrTiO3 thin film is insulating. *AIP Adv.* **2012**, *2*, No. 012147.

DOI: 10.1021/acsomega.8b01851
ACS Omega 2018, 3, 14266−14273